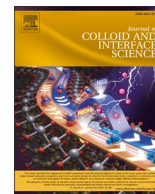


Contents lists available at [ScienceDirect](https://www.sciencedirect.com)

Journal of Colloid And Interface Science

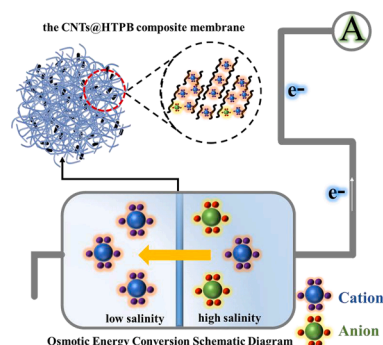
journal homepage: www.elsevier.com/locate/jcis

A facile strategy for the preparation of carbon nanotubes/polybutadiene crosslinked composite membrane and its application in osmotic energy harvesting

Cuncai Lin, Jinlin Hao, Jiawei Zhao, Yushuang Hou, Shuhui Ma, Xin Sui*

College of Materials Science and Engineering, Qingdao University, Qingdao, China

GRAPHICAL ABSTRACT



ARTICLE INFO

Keywords:

CNTs
Polybutadiene
Ion selectivity
Nanofluidic
Osmotic energy

ABSTRACT

The osmotic energy between riverine water and seawater can be converted into electricity by reverse electro-dialysis (RED). However, the facile fabrication of advanced RED membranes with high energy conversion efficiencies, large areas, and excellent mechanical properties remains a challenge. Carbon nanotubes (CNTs) exhibit excellent conductivity and provide suitable channels for ion transport but cannot form membranes independently, which limits the related applications in osmotic energy conversion. Herein, a new organic–inorganic composite membrane is prepared by combining hydroxyl-terminated polybutadiene as a matrix and carbon nanotubes as transport nanochannels. The nanotubes are pre-subjected to plasma treatment to increase the surface charge density and transport capacity of the nanochannels, improving the ion selectivity and energy conversion efficiency. Under actual seawater/river water conditions, the developed membrane delivers a power density of $\sim 5.1 \text{ W/m}^2$ and shows good mechanical strength (219 MPa). Our work provides a facile solution to the problem posed by the inability of ideal nanochannels to form membranes independently and paves the way for the application of RED membranes in osmotic energy conversion.

* Corresponding author.

E-mail address: suixin_1991@126.com (X. Sui).

<https://doi.org/10.1016/j.jcis.2023.10.084>

Received 16 September 2023; Received in revised form 10 October 2023; Accepted 17 October 2023

Available online 24 October 2023

0021-9797/© 2023 Elsevier Inc. All rights reserved.

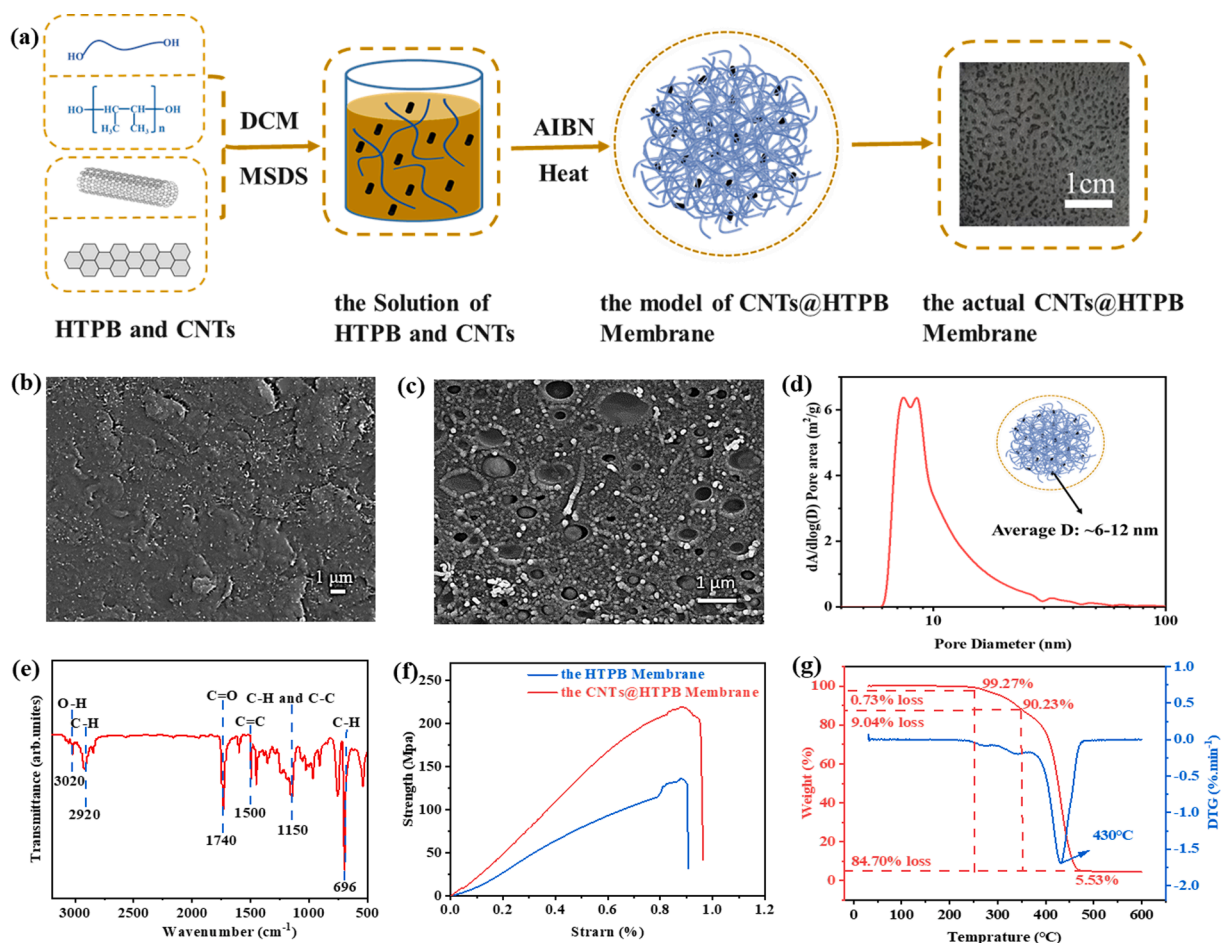


Fig. 1. Preparation process and characterizations of the CNTs@HTPB composite membrane. (a) Preparation process of CNTs@HTPB composite membrane. (b, c) Surface and cross-sectional SEM images of the CNTs@HTPB composite membrane, respectively. (d) Pore size distribution of the CNTs@HTPB composite membrane derived from BET. (e) FTIR spectrum of the CNTs@HTPB composite membrane. (f) Tensile strength curves of the CNTs@HTPB composite membrane, the stress constant is 1000.0 Pa/N, the strain constant is 1000.0 m⁻¹, and the zero reference position is 28.683 mm. (g) TGA and relevant DTG curves of the CNTs@HTPB composite membrane. Heating speed is 10 °C/min, stop temperature is 600 °C, and burning in argon gas.

1. Introduction

Osmotic energy is produced by the difference in salinity between different aqueous media (e.g., seawater and freshwater) [1–6] and can be converted into electrical energy through reverse electrodialysis (RED) [7–9], which relies on high-performance ion-selective membranes as the core component [10]. Furthermore, nano-ion channels are the key to ion-selective membranes, the rational design of nano-ion channels with high ion-selectivity is a prerequisite for achieving efficient osmotic energy conversion [11]. Given that traditional membranes are of limited applicability because of their low output power density and high internal resistance [12–15], it's very urgent to develop those membranes featuring the advantages of high power density, ease of preparation, low resistance, and high mechanical strength. In this regard, bionic nanofluidic membranes inspired by biological nanofluidic channels have recently received widespread attention [16–20]. Such channels, wherein ions exhibit transport properties different from those in solution, can be prepared for energy conversion by imitating the power generation principle of electric eels [18,21]. The ion-transport performance of nanofluidic channels is related to their surface charge density, which, in turn, is positively correlated with ion selectivity [19,22]. However, despite the progress made in this field, the development of new ion-selective membranes offering the benefits of high mechanical strength, high power density, and convenient large-scale preparation remains challenging.

Carbon materials are widely used for nanofluidic channel

construction because of their low cost and ease of production [23–26]. Jin et al. developed a g-C₃N₄/CNF membrane for osmotic energy conversion [27], with the power density of 0.25 W/m². Graphene, as a star material with layered structure [28–30], has been used to form ion-transport channels through layer stacking. However, its application is limited by low surface charge densities and the difficulty of large-scale preparation [31]. To improve the osmotic energy conversion efficiency, we herein focused on carbon nanotubes (CNTs) [32–35], which feature delocalised π -bonds formed from the p-electrons of sp²-hybridised carbon atoms and thus exhibit better mechanical properties (e.g., higher modulus) than graphene oxide [36]. Furthermore, CNTs offer the advantages of high electrical conductivity, mechanical strength, and specific surface area while featuring a high density of oxygenated surface functional groups, thus exhibiting high ion capacity and containing rich channel surface charges. CNTs hold great promise for energy storage and conversion, catalysis, adsorption, and separation applications [37,38]. The pore size and surface chemical structure of CNTs have been the subject of extensive research, which has promoted their rapid development and resulted in great application prospects [39]. However, the application of CNTs is limited by their inability to form membranes independently.

Hydroxyl-terminated polybutadiene (HTPB), a liquid pre-polymer developed in the 1960s, can be made into an elastomer with a three-dimensional network structure through chain extension and cross-linking curing reactions [40]. The cured product is an ideal membrane matrix as its excellent mechanical properties, particularly hydrolysis

resistance, acid and alkali resistance, wear resistance, low-temperature resistance, and good electrical insulation performance. Therefore, the hybridisation of CNTs with HTPB seems to be an effective route to high-performance RED membranes. Herein, we develop a simple and universal method that is suitable for the large-scale fabrication of composite membranes with high mechanical strength and output power density and can solve the problems posed by the inability of some precursor nanochannels to independently form membranes. Specifically, HTPB (matrix) and plasma-treated CNTs (ion-transport channels) are cross-linked at a controlled HTPB:CNT ratio to afford a CNT@HTPB composite membrane with high mechanical strength (219 MPa), conductivity, and cation selectivity. The end groups of HTPB chains and the carboxyl groups of CNTs can be ionised to charge the composite membrane and thus form the basis of its ion selectivity and energy conversion performance. In a simulated seawater/river water environment, the developed membrane exhibits an excellent energy conversion performance, delivering a power density of $\sim 4.2 \text{ W/m}^2$ that can be increased to 23.3 W/m^2 using a 500:1. The simplicity and upscalability of the membrane preparation process provide a basis for industrial applications and the fabrication of membranes intended for permeation energy conversion and ion screening.

2. Chemicals and materials

Hydroxyl-terminated polybutadiene ($M_n = 3088\text{--}4600$, Purity: $> 99\%$) was purchased from Energy Chemical. Trimethylol propane tris(3-mercaptopropionate) ($M_w = 398.56$, Purity: $> 85\%$) was purchased from Energy Chemical. The --COOH Functionalized and Multi-walled carbon nanotubes (OD: 5–15 nm, Length: 10–30 μm , Purity: $> 99\%$) were purchased from Time Nano. The Rhodamine 6G (Purity: $> 95\%$) and the fluorescein sodium salt (Purity: $> 70\%$) were purchased from Energy Chemical. Azobisisobutyronitrile (AIBN, Purity: $> 99\%$) was purchased from Chemical Book. Dichloromethane (Purity: $> 99.5\%$), NaCl, KCl, LiCl, CaCl_2 , MgCl_2 , HCl, and NaOH were all analytical grade and purchased from Sinopharm Chemical Reagent, China. These reagents were directly used without any purification.

2.1. Preparation of the CNTs@HTPB composite membrane

We use HTPB as the matrix, plasma treated carbon nanotubes for nanofluidic channels to prepare the composite membrane (Fig. 1(a)). In the preparation process, firstly, the hydroxyl-terminated polybutadiene was dissolved in dichloromethane (DCM), then, the trimethylol propane tris(3-mercaptopropionate), the plasma treated carbon nanotubes were mixed with azodiisobutyronitrile (AIBN) for ultrasonic treatment, then heating the solution to cross-link HTPB into network, finally, the CNTs@HTPB membrane was obtained by extrusion.

2.2. Characterization

The morphology of the CNTs@HTPB membrane was observed by a JSM-7800F scanning electron microscope (SEM, JEOL, Tokyo). The contact angle was measured through an optical contact angle measuring instrument (Theta, Biolin). The zeta potentials were measured using a solid surface zeta potential analyser (Anton Parr SurPASS). The ionic permeabilities of rhodamine 6G and fluorescein sodium salt were measured by a fluorescence spectrophotometer (Horiba X). Positively charged rhodamine 6G ($\text{Rh}(+)$) and negatively charged fluorescein sodium ($\text{Rh}(-)$) were used as the cation- and anion-selective probes respectively. The feed solution ($1 \times 10^{-5} \text{ M}$ fluorescent solution) and draw solution (deionized water) were separated with the CNTs@HTPB membrane in the electrochemical cell. The charged fluorescent dyes, $\text{Rh}(+)$ or $\text{Rh}(-)$, migrated following the concentration gradient. The concentration of the fluorescent dyes on the draw solution side was monitored by fluorescence spectroscopy. The electrical measurements were recorded with a Keithley6487 semiconductor pico-ammeter. the

CNTs@HTPB membrane was mounted between two cell conductance units filled with the test solution. A pair of self-made Ag/AgCl electrodes were placed on both sides of the conductivity cell to detect the trans-membrane potential. For energy conversion, an external resistor was connected to an electrochemical cell. As the resistance changed, the current was recorded with the pico-ammeter. For the I - V test, with the pico ammeter scanning function, the scanning interval was -0.2 V to 0.2 V or -2 V to 2 V , and the step voltage was 0.01 V or 0.1 V , to obtain the I - V curves of the membrane.

2.3. Calculating equations

2.3.1. Ion selectivity of the CNTs@HTPB membrane

The transference number τ_+ is calculated following the equation (1) [12,41,42].

$$\tau_+ = 1/2 \left\{ \frac{U_{diff}}{\frac{RT}{zF} \ln \frac{\lambda_{C_H} C_H}{\lambda_{C_L} C_L}} + 1 \right\} \quad (1)$$

where τ_+ is the cation transference number, U_{diff} refers to the diffusion potential; R , T , z , and F , refer to the gas constant, temperature, valence charge and Faraday constant respectively, λ , and c refer to ion activity coefficient and concentration.

2.3.2. Electrochemical energy conversion efficiency of the CNTs@HTPB membrane

Energy conversion efficiency is defined as the ratio of the output energy (electrical energy) to the input energy (Gibbs free energy of mixing), the efficiency corresponding to the maximum power generation, η_{max} is defined as equation (2) [12,43].

$$\eta_{max} = (2\tau_n - 1)^2/2 \quad (2)$$

3. Results and discussion

3.1. Characterisation of CNT@HTPB membrane

The synthesis of the CNT@HTPB membrane is illustrated in Fig. 1(a), with blue and black lines representing HTPB and CNTs, respectively. The HTPB matrix is formed by chemical cross-linking and combines with CNTs under the action of intermolecular forces and hydrogen bonds. Scanning electron microscopy (SEM) imaging showed the presence of nanofluidic channels (CNTs) independently leaked on the membrane surface (Fig. 1(b)) and uniformly distributed throughout the membrane (Fig. 1(c)). BET analysis showed that the membrane pores had sizes of 6–12 nm, in line with pure CNTs (Fig. 1(d)). Fourier transform infrared (FTIR) spectra featured peaks attributable to hydroxyl groups (3020 cm^{-1}), alkene $\text{C}=\text{C}$ bonds (1500 cm^{-1}), $\text{C}=\text{O}$ bonds (1740 cm^{-1}), and aromatic $\text{C}-\text{H}$ bonds in benzene rings (Fig. 1(e)). Thus, the CNT@HTPB membrane featured abundant terminal hydroxyl groups, which provide cation selectivity. The introduction of CNTs into HTPB increased membrane strength from ~ 120 to 219 MPa (Fig. 1(f)), possibly because of hydrogen bonding between these constituents [13,44]. The thermal stability of the CNT@HTPB membrane was probed by thermogravimetry-derivative thermogravimetry [45,46]. Weight loss occurred in three steps corresponding to the evaporation of absorbed water and residual organic solvents ($100\text{--}240 \text{ }^\circ\text{C}$), pyrolysis of oxygenated functional groups ($240\text{--}342 \text{ }^\circ\text{C}$), and the decomposition of HTPB ($342\text{--}470 \text{ }^\circ\text{C}$) (Fig. 1(g)). The decomposition temperature of the composite membrane was about $240 \text{ }^\circ\text{C}$. Thus, the CNT@HTPB membrane was thermally stable below $240 \text{ }^\circ\text{C}$, which is important for its applications.

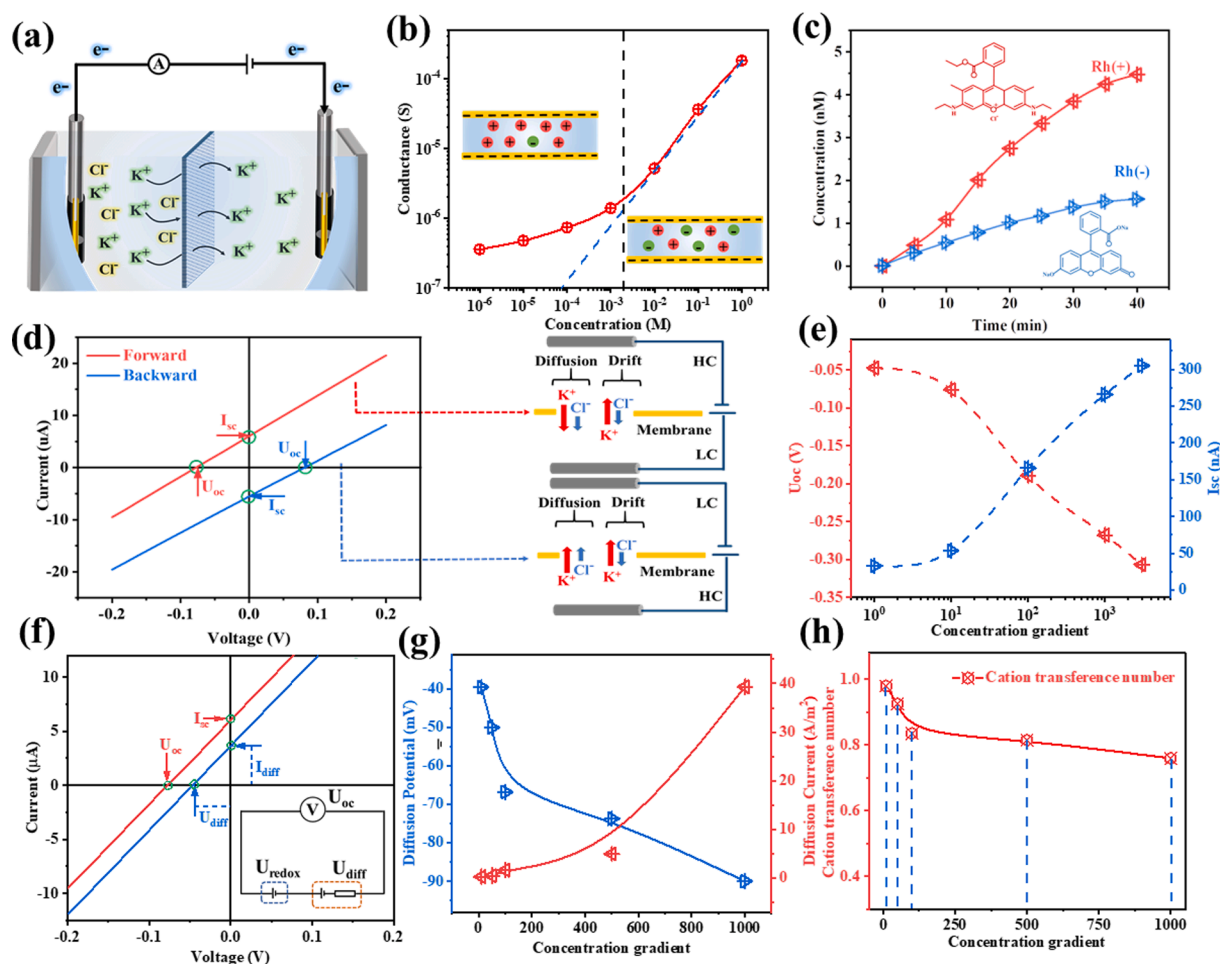


Fig. 2. Ion-transport properties of the CNT@HTPB membrane. (a) Ion-transport measurement diagram. (b) Ionic conductivity of the CNT@HTPB membrane as a function of KCl concentration. (c) Concentration of fluorescent dyes permeating through the membrane as a function of time. (d) Forward- and reverse-diffusion I - V curves of the CNT@HTPB membrane measured at a concentration gradient of $50\times$ (low-concentration side: $[KCl] = 0.01$ M). Arrows point to the corresponding experimental diagrams. (e) Open-circuit voltage and short-circuit current of the CNT@HTPB membrane as functions of the concentration gradient. (f) Open-circuit potential and diffusion potential generated by the CNT@HTPB membrane. The illustration schematically depicts the potential composition of the experimental device. (g) Diffusion potential and diffusion current of the CNT@HTPB membrane as functions of the concentration gradient ($[KCl] = 0.00001$ M at low-concentration-side). (h) Ion mobility of the CNT@HTPB membrane as a function of the concentration gradient.

3.2. Ion-transport properties of CNT@HTPB membrane

The ion-transport properties of the CNT@HTPB membrane were tested using KCl as a representative electrolyte because of the very similar bulk mobilities of K^+ and Cl^- ions. The membrane (testing area ≈ 0.0314 mm²) was sandwiched in a double-chamber electrolytic cell, and voltage was applied using a pair of Ag/AgCl electrodes (Fig. 2(a)) to measure ionic conductance at different KCl concentrations (Fig. 2(b)). At $[KCl] < 0.009$ M, the ionic conductance was subject to deviation, as it was no longer determined by the electrolyte concentration but was rather influenced by the effects of electric double layers (EDLs) on the membrane [47,48]. In the high-concentration region, the EDL thickness (λ_D) was smaller than the average channel size, leading to bulk ion diffusion. In the low-concentration region, λ_D was close to the channel diameter, resulting in EDL overlap. Under this condition, ion transport was controlled by surface charge. To examine the ion selectivity of the CNTs@HTPB membrane, we selected two fluorescent dyes with different charges, namely the positively charged rhodamine 6G and the negatively charged fluorescein sodium (red and blue lines in Fig. 2(c), respectively). The transmittance of rhodamine 6G substantially exceeded that of fluorescein sodium under the same conditions, which indicated that the CNT@HTPB membrane featured high cation selectivity, in line with the abundant carboxyl groups in the membrane channels.

The I - V curve of the CNT@HTPB membrane was recorded under forward and reverse voltage scanning from -0.2 to 0.2 V. The forward and reverse I - V curves were symmetrical about the origin, indicating that the nanofluidic channels on the CNT@HTPB membrane were also symmetrical (Fig. 2(d)). U_{oc} consists of two parts, namely the oxidation–reduction potential (U_{redox}) generated by the unequal potential at the electrode–solution interface at different electrolyte concentrations and the diffusion potential (U_{diff}) contributed by the membrane [12,49]. Under a concentration gradient, the ions spontaneously diffuse through the CNT@HTPB membrane towards the low-concentration side. The diffusion current (I_{diff}) is generated by the separation of cations and anions in the EDL on the inner walls of the nanofluidic channels, which can be explained using Poisson and Nernst–Planck equations [50]. The open-circuit voltage U_{oc} (potential at zero current) and short-circuit current I_{sc} (current at zero external voltage) were measured for different concentration gradients (0.001 M KCl on the low-concentration side) and shown to be positively correlated with the latter parameter (Fig. 2(e)). With an increase in the salinity gradient between the two sides of the membrane, the ion transmembrane thrust increased, and the cations in the solution on the high-concentration side were more easily transferred to the low-concentration side.

To study the actual diffusion voltage of the CNT@HTPB membrane, we measured U_{diff} and I_{diff} (Fig. 2(f)). In this figure, the red line

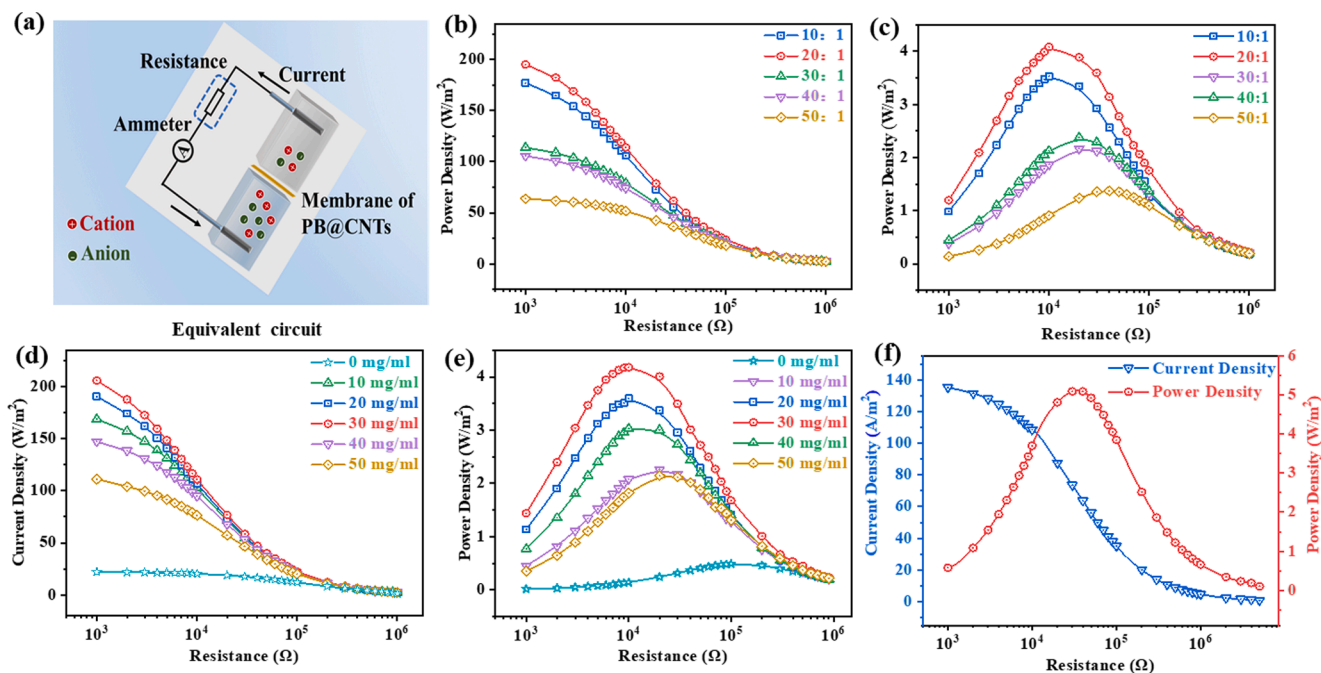


Fig. 3. Osmotic energy conversion performance of the CNT@HTPB membrane-based power generator. (a) Equivalent circuit diagram used to quantify the efficiency of osmotic energy conversion. Red and green spheres indicate cations and anions, respectively. (b) Current density and (c) power density as functions of the HTPB: CNT ratio. (d) Current density and (e) power density as functions of the concentration of CNTs in DCM at a fixed HTPB:CNT ratio of 20:1. (f) Current density (blue) and power (red) densities of the CNT@HTPB membrane observed for actual seawater/river water, the seawater comes from the Wheat Island area in the southern district of Qingdao City, China, and the river water comes from the tap water of Qingdao, China. (For interpretation of the references to colour in this figure legend, the reader is referred to the web version of this article.)

represents the *I-V* curve produced under the action of ion diffusion and electrode oxidation–reduction, while the blue line represents the curve produced under the action of ion diffusion only. In the case of the red

line, the *x*-axis intercept corresponds to the open-circuit potential (80.97 mV), and the *y*-axis intercept corresponds to the short-circuit current (5.61 μ A). In the case of the blue line, the *x*-axis intercept

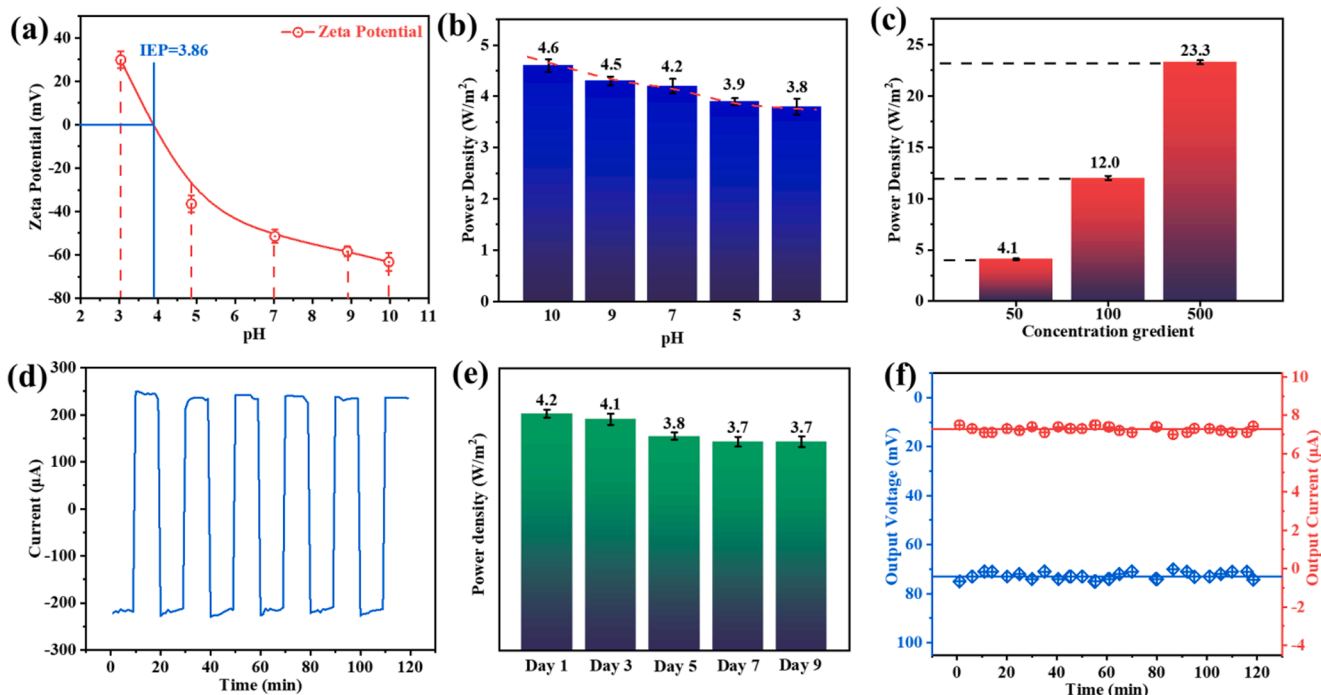


Fig. 4. Environmental influence and stability of the CNT@HTPB membrane. (a) Zeta potential and (b) power density with different pH values. (c) Power density as a function of the salinity gradient ($[KCl] = 0.01$ M on one side and 0.5, 1.0, or 5.0 M on the other side; error bars represent standard deviations). (d) Output current versus time curve recorded upon voltage cycling from -2 to $+2$ V. (e) Power density delivered by the CNT@HTPB membrane as a function of time (error bars represent standard deviations). (f) Output current and output voltage as functions of time under simulated seawater conditions ($[KCl] = 0.01$ M on one side and 0.5 M on the other side).

corresponds to the diffusion potential (53.57 mV), and the y-axis intercept corresponds to the diffusion current (3.34 μA). Next, we examined changes in the diffusion potential and diffusion current of the CNT@HTPB membrane under different concentration gradients. The concentration of KCl on the low-concentration side was fixed, and that on the high-concentration side was varied. With the increasing concentration gradient, the electromotive force of diffusion increased from 39.5 to 89.97 mV, and the diffusion current density increased from 0.25 to 39.3 A/m^2 (Fig. 2(g)). The cationic mobility of the CNT@HTPB membrane was determined (Eq. (1)) under different concentration gradients produced at a fixed KCl concentration of 0.00001 M at the low-concentration side and varied KCl concentration at the high-concentration side and was shown to be negatively correlated with this gradient (Fig. 2(h)). At $C_{\text{high}}/C_{\text{low}} = 1000$, τ_+ was still close to 0.8, i. e., the CNT@HTPB membrane retained high cationic mobility [41,48,51].

3.3. Osmotic energy conversion performance of CNT@HTPB membrane

To investigate the osmotic energy conversion performance of the CNT@HTPB membrane, we added an external resistance (R_L) to the membrane-based generator and calculated the output power as $P = I^2 R_L$, where I is the generated current. As the ionic diffusion coefficient of K^+ ions is similar to that of Cl^- ions, we aqueous KCl to simulate seawater and river water. The equivalent circuit diagram used for these electrochemical measurements is shown in Fig. 3(a). KCl concentrations at low- and high-concentration sides were fixed at 0.01 and 0.5 M, respectively. Several membranes were prepared to examine the effects of membrane composition and CNT concentration on energy conversion performance. Initially, the CNT concentration was fixed, and membranes with different HTPB:CNT ratios were prepared. With an increase in this ratio, the membrane current density decreased, and the membrane power density first increased and then decreased, peaking at a HTPB:CNT ratio of 20:1 (Fig. 3(b) and (c)). Next, the above ratio was fixed at 20:1, and the concentration of plasma-treated CNTs in DCM was varied. The highest power density was obtained at CNT concentration of 30 mg/mL (Fig. 3(d) and (e)). The maximal power density under optimised conditions (HTPB:CNT = 20:1, [CNTs] = 30 mg/mL) and an external resistance of 10 k Ω was 4.2 W/m^2 [5,52]. At a low CNT content, the nanofluidic channels in the HTPB matrix were scarce, and energy conversion performance was poor. However, at an overly high CNT content, the nanofluidic channels overlapped with each other, the internal resistance increased, and the energy-conversion performance deteriorated. Similarly, when the concentration of CNTs was overly high, the agglomeration of CNTs resulted in channel overlap and increased internal resistance. When the CNT concentration was overly low, the number of channels per membrane unit area was also low, and energy conversion performance was poor. Therefore, the CNT@HTPB membrane achieved the highest performance at HTPB:CNT ratio of 20:1 and a CNT concentration of 30 mg/mL. Finally, the osmotic energy conversion performance of the optimal CNTs@HTPB membrane was measured for seawater and river water samples (Fig. 3(f)). The maximum current and power densities were determined as 137.5 A/m^2 and 5.1 W/m^2 , respectively, indicating high osmotic energy conversion performance [52,53].

3.4. Test environment and stability of CNT@HTPB membrane

The osmotic energy conversion performance of the CNT@HTPB membrane was studied in different test environments [21,54,55]. Fig. 4 (a) shows the membrane zeta potential as a function of pH, showing that this potential equalled -46 mV at $\text{pH} \approx 7$. Thus, the membrane surface was negatively charged under neutral conditions. With an increase in pH, the zeta potential became more negative, and the isoelectric point was observed at $\text{pH} 3.86$. Moreover, cation selectivity and energy conversion efficiency increased with increasing pH (Fig. 4(b)), and high

energy conversion performance was retained over a wide pH range. Subsequently, the power density of the CNT@HTPB membrane was measured at different salinity gradients ($[\text{KCl}] = 0.01$ M on one side and 0.5, 1.0, or 5.0 M on the other side). As shown in Fig. 4(c), the maximum power density of 23.3 W/m^2 was achieved at a salinity gradient of 500 \times .

The generation of electricity from seawater and river water requires the membrane to be soaked in a solution for a long time [8,55], which indicates the importance of membrane stability. The membrane output current was measured under the cyclic scanning of voltage (+2 and -2 V) applied on both membrane sides at a cycling interval of 10 min and $[\text{KCl}] = 0.1$ M (Fig. 4(d)). The current at different polarity voltages remained stable for 120 min. Over several days, the power density of the CNT@HTPB membrane slightly decreased but remained high, indicating great stability (Fig. 4(e)). Finally, the output current and voltage were measured as functions of time (time interval = 5 min) under simulated seawater conditions (Fig. 4(f)) and were relatively stable within 120 min (output voltage = 74 mV, output current = 7.2 μA). This behaviour shows that the CNT@HTPB membrane exhibits excellent long-term stability and thus has great practical application prospects for osmotic energy conversion [12,56].

4. Conclusion

A new type of organic–inorganic composite membrane was prepared using HTPB as the matrix and carbon nanotubes as nanofluidic channels. Compared to traditional ion-exchange membranes, the CNT@HTPB membrane featured a high power density, easy preparation process, and ultrahigh mechanical strength. Most importantly, our work addresses the problem posed by the inability of CNTs to independently form membranes and describes the fabrication of ideal nanofluidic channels for RED. The developed strategy can be extended to other materials and paves the way for the development of new types of ion-selective membranes. In future work, the application of the CNT @ HTPB membrane in different energy conversion systems will be explored.

CRedit authorship contribution statement

Cuncai Lin: Formal analysis, Data curation, Investigation, Writing – original draft. **Jinlin Hao:** Data curation. **Jiawei Zhao:** Formal analysis. **Yushuang Hou:** Formal analysis. **Shuhui Ma:** Investigation. **Xin Sui:** Project administration, Writing – review & editing, Supervision.

Declaration of Competing Interest

The authors declare that they have no known competing financial interests or personal relationships that could have appeared to influence the work reported in this paper.

Data availability

Data will be made available on request.

Acknowledgements

The work was supported by the National Natural Science Foundation of China (No. 22005162) and the Natural Science Foundation of Shandong Province (No. ZR2020QE093).

References

- [1] R.E. Pattle, Production of electric power by mixing fresh and salt water in the hydroelectric pile, 660–660, *Nature* 174 (4431) (1954), <https://doi.org/10.1038/174660a0>.
- [2] Z. Zhang, L. He, C.C. Zhu, Y.C. Qian, L.P. Wen, L. Jiang, Improved osmotic energy conversion in heterogeneous membrane boosted by three-dimensional hydrogel

- interface, *Nat. Commun.* 11 (1) (2020) 8, <https://doi.org/10.1038/s41467-020-14674-6>.
- [3] Z. Zhang, X. Sui, P. Li, G.H. Xie, X.Y. Kong, K. Xiao, L.C. Gao, L.P. Wen, L. Jiang, Ultrathin and ion-selective janus membranes for high-performance osmotic energy conversion, *J. Am. Chem. Soc.* 139 (26) (2017) 8905–8914, <https://doi.org/10.1021/jacs.7b02794>.
- [4] Z. Zhang, L.P. Wen, L. Jiang, Nanofluidics for osmotic energy conversion, *Nat. Rev. Mater.* 6 (7) (2021) 622–639, <https://doi.org/10.1038/s41578-021-00300-4>.
- [5] L. Ding, D. Xiao, Z. Lu, J.J. Deng, Y.Y. Wei, J. Caro, H.H. Wang, Oppositely charged $\text{Ti}_3\text{C}_2\text{Tx}$ MXene membranes with 2D nanofluidic channels for osmotic energy harvesting, *Angew. Chem. Int. Ed.* 59 (22) (2020) 8720–8726, <https://doi.org/10.1002/anie.201915993>.
- [6] Z.T. Wu, T. Zhang, B.X. Wang, P. Ji, N. Sheng, M.H. Zhang, Q.Q. Liang, S.Y. Chen, H.P. Wang, Scalable bacterial cellulose biofilms with improved ion transport for high osmotic power generation, *Nano Energy* 88 (2021) 8, <https://doi.org/10.1016/j.nanoen.2021.106275>.
- [7] K.T. Huang, W.H. Hung, Y.C. Su, F.C. Tang, L.D. Linh, C.J. Huang, L.H. Yeh, Zwitterionic gradient double-network hydrogel membranes with superior biofouling resistance for sustainable osmotic energy harvesting, *Adv. Funct. Mater.* (2023), <https://doi.org/10.1002/adfm.202211316>.
- [8] Q. Luo, P. Liu, L. Fu, Y. Hu, L. Yang, W. Wu, X.Y. Kong, L. Jiang, L. Wen, Engineered cellulose nanofiber membranes with ultrathin low-dimensional carbon material layers for photothermal-enhanced osmotic energy conversion, *ACS Appl. Mater. Interfaces* 14 (11) (2022) 13223–13230, <https://doi.org/10.1021/acsaami.1c22707>.
- [9] Z. Zhang, P. Bhauriyal, H. Sahabudeen, Z. Wang, X. Liu, M. Hamsch, S.C. B. Mansfeld, R. Dong, T. Heine, X. Feng, Cation-selective two-dimensional polyimine membranes for high-performance osmotic energy conversion, *Nature, Communications* 13 (1) (2022), <https://doi.org/10.1038/s41467-022-31523-w>.
- [10] Q. Ren, K. Chen, H. Zhu, J.F. Zhang, Z.G. Qu, Nanoparticle enhanced salinity-gradient osmotic energy conversion under photothermal effect, *Energ. Convers. Manage.* 251 (2022), <https://doi.org/10.1016/j.enconman.2021.115032>.
- [11] C. Li, L.C. Gao, Specific ion selectivity with a reverse-selective mechanism, *Nat. Nanotechnol.* 17 (11) (2022) 1130–1131, <https://doi.org/10.1038/s41565-022-01216-y>.
- [12] L. Ding, D. Xiao, Z. Zhao, Y. Wei, J. Xue, H. Wang, Ultrathin and ultrastrong Kevlar aramid nanofiber membranes for highly stable osmotic energy conversion, *Adv. Sci.* 9 (25) (2022), <https://doi.org/10.1002/advs.202202869>.
- [13] C. Li, L.P. Wen, X. Sui, Y.R. Cheng, L.C. Gao, L. Jiang, Large-scale, robust mushroom-shaped nanochannel array membrane for ultrahigh osmotic energy conversion, *Sci. Adv.* 7 (21) (2021) 7, <https://doi.org/10.1126/sciadv.abg2183>.
- [14] Y.C. Liu, L.H. Yeh, M.J. Zheng, K.C.W. Wu, Highly selective and high-performance osmotic power generators in subnanochannel membranes enabled by metal-organic frameworks, *Sci. Adv.* 7 (10) (2021) 9, <https://doi.org/10.1126/sciadv.abe9924>.
- [15] X. Li, P. Cheng, J.K. Zhang, H. Nawaz, Y.L. Xu, F. Xu, Laminar regenerated cellulose membrane employed for high-performance photothermal-gating osmotic power harvesting, *Carbohydr. Polym.* 292 (2022) 11, <https://doi.org/10.1016/j.carbpol.2022.119657>.
- [16] Y.P. Feng, W.W. Zhu, W. Guo, L. Jiang, Bioinspired energy conversion in nanofluidics: a paradigm of material evolution, *Adv. Mater.* 29 (45) (2017) 8, <https://doi.org/10.1002/adma.201702773>.
- [17] B.E. Logan, M. Elimelech, Membrane-based processes for sustainable power generation using water, *Nature* 488 (7411) (2012) 313–319, <https://doi.org/10.1038/nature11477>.
- [18] Y.D. Wu, W.W. Xin, X.Y. Kong, J.J. Chen, Y.C. Qian, Y. Sun, X.L. Zhao, W.P. Chen, L. Jiang, L.P. Wen, Enhanced ion transport by graphene oxide/cellulose nanofibers assembled membranes for high-performance osmotic energy harvesting, *Mater. Horiz.* 7 (10) (2020) 2702–2709, <https://doi.org/10.1039/d0mh00979b>.
- [19] Y. Xu, Nanofluidics: A new arena for materials science, *Adv. Mater.* 30 (3) (2018) 17, <https://doi.org/10.1002/adma.201702419>.
- [20] L. Zhang, X.A. Kan, T. Huang, J.C. Lao, K.G. Luo, J. Gao, X.L. Liu, K.Y. Sui, L. Jiang, Electric field modulated water permeation through laminar $\text{Ti}_3\text{C}_2\text{Tx}$ MXene membrane, *Water Res.* 219 (2022) 7, <https://doi.org/10.1016/j.watres.2022.118598>.
- [21] M.J. Esplandiú, D. Reguera, D. Romero-Guzman, A.M. Gallardo-Moreno, J. Fraxedas, From radial to unidirectional water pumping in zeta-potential modulated Nafion nanostructures, *Nat. Commun.* 13 (1) (2022), <https://doi.org/10.1038/s41467-022-30554-7>.
- [22] X. Zuo, C. Zhu, W. Xian, Q.W. Meng, Q. Guo, X. Zhu, S. Wang, Y. Wang, S. Ma, Q. Sun, Thermo-osmotic energy conversion enabled by covalent-organic-framework membranes with record output power density, *Angew. Chem. Int. Ed.* 61 (18) (2022), <https://doi.org/10.1002/anie.202116910>.
- [23] L. Fu, S. Merabia, L. Joly, Understanding fast and robust thermo-osmotic flows through carbon nanotube membranes: thermodynamics meets hydrodynamics, *J. Am. Chem. Soc.* 9 (8) (2018) 2086–2092, <https://doi.org/10.1021/acs.jpcclett.8b00703>.
- [24] L. Xie, S. Zhou, J.R. Liu, B.L. Qiu, T.Y. Liu, Q.R. Liang, X.Z. Zheng, B. Li, J. Zeng, M. Yan, Y.J. He, X. Zhang, H. Zeng, D. Ma, P. Chen, K. Liang, L. Jiang, Y. Wang, D. Y. Zhao, B.A. Kong, Sequential superassembly of nanofiber arrays to carbonaceous ordered mesoporous nanowires and their heterostructure membranes for osmotic energy conversion, *J. Am. Chem. Soc.* 143 (18) (2021) 6922–6932, <https://doi.org/10.1021/jacs.1c00547>.
- [25] Z.K. Zhang, W.H. Shen, L.X. Lin, M. Wang, N. Li, Z.F. Zheng, F. Liu, L.X. Cao, Vertically transported graphene oxide for high-performance osmotic energy conversion, *Adv. Sci.* 7 (12) (2020) 8, <https://doi.org/10.1002/advs.202000286>.
- [26] Y.L. Tan, C.X. Yang, W.W. Qian, C. Teng, Flower-like MnO_2 on layered carbon derived from sisal hemp for asymmetric supercapacitor with enhanced energy density, *J. Alloy. Compd.* 826 (2020) 9, <https://doi.org/10.1016/j.jallcom.2020.154133>.
- [27] Z.X. Gao, Z. Sun, M. Ahmad, Y.Q. Liu, H.Y. Wei, S. Wang, Y.C. Jin, Increased ion transport and high-efficient osmotic energy conversion through aqueous stable graphitic carbon nitride/cellulose nanofiber composite membrane, *Carbohydr. Polym.* 280 (2022) 8, <https://doi.org/10.1016/j.carbpol.2021.119023>.
- [28] M.R. Karim, K. Hatakeyama, T. Matsui, H. Takehira, T. Taniguchi, M. Koinuma, Y. Matsumoto, T. Akutagawa, T. Nakamura, S. Noro, T. Yamada, H. Kitagawa, S. Hayami, Graphene oxide nanosheet with high proton conductivity, *J. Am. Chem. Soc.* 135 (22) (2013) 8097–8100, <https://doi.org/10.1021/ja401060q>.
- [29] J. Tang, Q. Chen, L.G. Xu, S. Zhang, L.Z. Feng, L. Cheng, H. Xu, Z. Liu, R. Peng, Graphene oxide-silver nanocomposite as a highly effective antibacterial agent with species-specific mechanisms, *ACS Appl. Mater. Interfaces* 5 (9) (2013) 3867–3874, <https://doi.org/10.1021/am4005495>.
- [30] F.K. Wang, Z.Y. Wang, S.D. Wang, X.X. Meng, Y. Jin, N.T. Yang, J. Sunarso, S. M. Liu, Mechanically intensified and stabilized MXene membranes via the combination of graphene oxide for highly efficient osmotic power production, *J. Membr. Sci.* 647 (2022) 10, <https://doi.org/10.1016/j.memsci.2022.120280>.
- [31] K.R. Bang, C. Kwon, H. Lee, S. Kim, E.S. Cho, Horizontally asymmetric nanochannels of graphene oxide membranes for efficient osmotic energy harvesting, *ACS Nano* (2023), <https://doi.org/10.1021/acsnano.2c11975>.
- [32] R.P. Fang, K. Chen, L.C. Yin, Z.H. Sun, F. Li, H.M. Cheng, The regulating role of carbon nanotubes and graphene in lithium-ion and lithium-sulfur batteries, *Adv. Mater.* 31 (9) (2019) 22, <https://doi.org/10.1002/adma.201800863>.
- [33] S. Kumar, R. Rani, N. Dilbaghi, K. Tanqueswar, K.H. Kim, Carbon nanotubes: a novel material for multifaceted applications in human healthcare, *Chem. Soc. Rev.* 46 (1) (2017) 158–196, <https://doi.org/10.1039/c6cs00517a>.
- [34] H. Omachi, Y. Segawa, K. Itami, Synthesis of Cycloparaphenylenes and related carbon nanorings: a step toward the controlled synthesis of carbon nanotubes, *Acc. Chem. Res.* 45 (8) (2012) 1378–1389, <https://doi.org/10.1021/ar300055x>.
- [35] B.S. Wong, S.L. Yoong, A. Jagusiak, T. Pancyk, H.K. Ho, W.H. Ang, G. Pastorin, Carbon nanotubes for delivery of small molecule drugs, *Adv. Drug Deliv. Rev.* 65 (15) (2013) 1964–2015, <https://doi.org/10.1016/j.addr.2013.08.005>.
- [36] C.W. Mao, Y.X. Chang, X.T. Zhao, X.Y. Dong, Y.F. Geng, N. Zhang, L. Dai, X.W. Wu, L. Wang, Z.X. He, Functional carbon materials for high-performance Zn metal anodes, *J. Energy Chem.* 75 (2022) 135–153, <https://doi.org/10.1016/j.ijechem.2022.07.0342095-4956>.
- [37] Y.B. Liu, G.D. Gao, C.D. Vecitis, Prospects of an electroactive carbon nanotube membrane toward environmental applications, *Acc. Chem. Res.* 53 (12) (2020) 2892–2902, <https://doi.org/10.1021/acs.accounts.0c00544>.
- [38] L. Wen, F. Li, H.M. Cheng, Carbon nanotubes and graphene for flexible electrochemical energy storage: from materials to devices, *Adv. Mater.* 28 (22) (2016) 4306–4337, <https://doi.org/10.1002/adma.201504225>.
- [39] S. Mallakpour, E. Khadem, Carbon nanotube-metal oxide nanocomposites: fabrication, properties and applications, *Chem. Eng. J.* 302 (2016) 344–367, <https://doi.org/10.1016/j.cej.2016.05.038>.
- [40] R. Thomas, D. Yumei, H. Yuelong, Y. Le, P. Moldenaers, Y. Weimin, T. Czigan, S. Thomas, Miscibility, morphology, thermal, and mechanical properties of a DGEBA based epoxy resin toughened with a liquid rubber, *Polymer* 49 (1) (2008) 278–294, <https://doi.org/10.1016/j.polymer.2007.11.030>.
- [41] X.H. Zuo, C.J. Zhu, W.P. Xian, Q.W. Meng, Q. Guo, X.C. Zhu, S. Wang, Y.Q. Wang, S.Q. Ma, Q. Sun, Thermo-osmotic energy conversion enabled by covalent-organic-framework membranes with record output power density, *Angew. Chem. Int. Ed.* 61 (18) (2022) 8, <https://doi.org/10.1002/anie.202116910>.
- [42] V.P. Mai, R.J. Yang, Boosting power generation from salinity gradient on high-density nanoporous membrane using thermal effect, *Appl. Energy* 274 (2020) 9, <https://doi.org/10.1016/j.apenergy.2020.115294>.
- [43] W. Xin, Z. Zhang, X. Huang, Y. Hu, T. Zhou, C. Zhu, X.-Y. Kong, L. Jiang, L. Wen, High-performance silk-based hybrid membranes employed for osmotic energy conversion, *Nat. Commun.* 10 (2019), <https://doi.org/10.1038/s41467-019-11792-8>.
- [44] W.J. Wang, J.L. Hao, Q. Sun, M.Q. Zhao, H.Y. Liu, C. Li, X. Sui, Carbon nanofibers membrane bridged with graphene nanosheet and hyperbranched polymer for high-performance osmotic energy harvesting, *Nano Res.* 16 (1) (2023) 1205–1211, <https://doi.org/10.1007/s12274-022-4634-6>.
- [45] A. Alkhouzaam, H. Qiblawey, M. Khraishah, Polydopamine functionalized graphene oxide as membrane nanofiller: spectral and structural studies, *Membranes* 11 (2) (2021) 17, <https://doi.org/10.3390/membranes11020086>.
- [46] J.L. Hao, Y.K. Ning, Y.S. Hou, S.H. Ma, C.C. Lin, J.W. Zhao, C. Li, X. Sui, Polydopamine functionalized graphene oxide membrane with the sandwich structure for osmotic energy conversion, *J. Colloid Interf. Sci.* 630 (2023) 795–803, <https://doi.org/10.1016/j.jcis.2022.10.084>.
- [47] K. Xiao, C.J. Wan, L. Jiang, X.D. Chen, M. Antonietti, Bioinspired ionic sensory systems: the successor of electronics, *Adv. Mater.* 32 (31) (2020) 9, <https://doi.org/10.1002/adma.202000218>.
- [48] Y.H. Zhou, L. Jiang, Bioinspired nanoporous membrane for salinity gradient energy harvesting, *Joule* 4 (11) (2020) 2244–2248, <https://doi.org/10.1016/j.joule.2020.09.009>.
- [49] M.C. Zhang, K.C. Guan, Y.F. Ji, G.P. Liu, W.Q. Jin, N.P. Xu, Controllable ion transport by surface-charged graphene oxide membrane, *Nat. Commun.* 10 (2019) 8, <https://doi.org/10.1038/s41467-019-09286-8>.
- [50] W. Guo, L.X. Cao, J.C. Xia, F.Q. Nie, W. Ma, J.M. Xue, Y.L. Song, D.B. Zhu, Y. G. Wang, L. Jiang, Energy harvesting with single-ion-selective nanopores: a

- concentration-gradient-driven nanofluidic power source, *Adv. Funct. Mater.* 20 (8) (2010) 1339–1344, <https://doi.org/10.1002/adfm.200902312>.
- [51] Z. Zhang, S. Yang, P.P. Zhang, J. Zhang, G.B. Chen, X.L. Feng, Mechanically strong MXene/Kevlar nanofiber composite membranes as high-performance nanofluidic osmotic power generators, *Nat. Commun.* 10 (2019) 9, <https://doi.org/10.1038/s41467-019-10885-8>.
- [52] S. Hong, F.W. Ming, Y. Shi, R.Y. Li, L.S. Kim, C.Y.Y. Tang, H.N. Alshareef, P. Wang, Two-dimensional Ti_3C_2Tx MXene membranes as nanofluidic osmotic power generators, *ACS Nano* 13 (8) (2019) 8917–8925, <https://doi.org/10.1021/acsnano.9b02579>.
- [53] J.F. Huang, M. Mensi, E. Oveisi, V. Mantella, R. Buonsanti, Structural sensitivities in bimetallic catalysts for electrochemical CO_2 reduction revealed by Ag-Cu nanodimers, *J. Am. Chem. Soc.* 141 (6) (2019) 2490–2499, <https://doi.org/10.1021/jacs.8b12381>.
- [54] X.M. Ding, Y.P. Pu, M. Tang, T. Zhang, Environmental and health effects of graphene-family nanomaterials: potential release pathways, transformation, environmental fate and health risks, *Nano Today* 42 (2022) 23, <https://doi.org/10.1016/j.nantod.2022.101379>.
- [55] J.G. Duan, Y.S. Li, Y.C. Pan, N. Behera, W.Q. Jin, Metal-organic framework nanosheets: an emerging family of multifunctional 2D materials, *Coordinat. Chem. Rev.* 395 (2019) 25–45, <https://doi.org/10.1016/j.ccr.2019.05.018>.
- [56] J.L. Yang, B. Tu, G.J. Zhang, P.C. Liu, K. Hu, J.R. Wang, Z. Yan, Z.W. Huang, M. N. Fang, J.J. Hou, Q.J. Fang, X.H. Qiu, L.S. Li, Z.Y. Tang, Advancing osmotic power generation by covalent organic framework monolayer, *Nat. Nanotechnol.* 17 (6) (2022) 622–+, <https://doi.org/10.1038/s41565-022-01110-7>.